

Review

Cascaded Generation in Multimode Diode-Pumped Graded-Index Fiber Raman Lasers

Alexey G. Kuznetsov¹, Ilya N. Nemov¹, Alexey A. Wolf¹ , Ekaterina A. Evmenova¹, Sergey I. Kablukov¹ 
and Sergey A. Babin^{1,2,*}

¹ Institute of Automation and Electrometry, Siberian Branch of the Russian Academy of Sciences, 1 Ac. Koptuyug Ave., 630090 Novosibirsk, Russia; KuznetsovAG@iae.nsk.su (A.G.K.); Nemov@iae.nsk.su (I.N.N.); wolf@iae.nsk.su (A.A.W.); Evmenova@iae.nsk.su (E.A.E.); kab@iae.nsk.su (S.I.K.)
² Physics Department, Novosibirsk State University, 2 Pirogova Str., 630090 Novosibirsk, Russia
* Correspondence: babin@iae.nsk.su

Abstract: We review our recent experimental results on the cascaded Raman conversion of highly multimode laser diode (LD) pump radiation into the first- and higher-order Stokes radiation in multimode graded-index fibers. A linear cavity composed of fiber Bragg gratings (FBGs) inscribed in the fiber core is formed to provide feedback for the first Stokes order, whereas, for the second order, both a linear cavity consisting of two FBGs and a half-open cavity with one FBG and random distributed feedback (RDFB) via Rayleigh backscattering along the fiber are explored. LDs with different wavelengths (915 and 940 nm) are used for pumping enabling Raman lasing at different wavelengths of the first (950, 954 and 976 nm), second (976, 996 and 1019 nm) and third (1065 nm) Stokes orders. Output power and efficiency, spectral line shapes and widths, beam quality and shapes are compared for different configurations. It is shown that the RDFB cavity provides higher slope efficiency of the second Stokes generation (up to 70% as that for the first Stokes wave) with output power up to ~30 W, limited by the third Stokes generation. The best beam quality parameter of the second Stokes beam is close to the diffraction limit ($M^2 \sim 1.3$) in both linear and half-open cavities, whereas the line is narrower (< 0.2 nm) and more stable in the case of the linear cavity with two FBGs. However, an optimization of the FBG reflection spectrum used in the half-open cavity allows this linewidth value to be approached. The measured beam profiles show the dip formation in the output pump beam profile, whereas the first and second Stokes beams are Gaussian-shaped and almost unchanged with increasing power. A qualitative explanation of such behavior in connection with the power evolution for the transmitted pump and generated first, second and third Stokes beams is given. The potential for wavelength tuning of the cascaded Raman lasers based on LD-pumped multimode fibers is discussed.



Citation: Kuznetsov, A.G.; Nemov, I.N.; Wolf, A.A.; Evmenova, E.A.; Kablukov, S.I.; Babin, S.A. Cascaded Generation in Multimode Diode-Pumped Graded-Index Fiber Raman Lasers. *Photonics* **2021**, *8*, 447. <https://doi.org/10.3390/photonics8100447>

Received: 21 September 2021

Accepted: 11 October 2021

Published: 15 October 2021

Publisher's Note: MDPI stays neutral with regard to jurisdictional claims in published maps and institutional affiliations.



Copyright: © 2021 by the authors. Licensee MDPI, Basel, Switzerland. This article is an open access article distributed under the terms and conditions of the Creative Commons Attribution (CC BY) license (<https://creativecommons.org/licenses/by/4.0/>).

Keywords: fiber laser; Raman laser; cascaded; multimode; graded-index; diode pumping; brightness enhancement; beam quality; wavelength agile

1. Introduction

Raman fiber lasers (RFL) are known as wavelength-agile laser sources utilizing almost all the advantages of fiber lasers, such as high efficiency, beam quality and stability, in a reliable, adjustment-free, all-fiber cavity; see [1,2] for a review. At appropriate optical pumping, conventional telecom passive fibers become an amplifying medium due to the effect of stimulated Raman scattering (SRS). A broad SRS bandwidth extended up to several tens of THz from the pump wavelength and higher-order SRS at high-power pumping enable Raman generation at almost any wavelength in a transparency window of silica-based fibers ranging from ~1 to ~2 μm when pumped by a high-power Yb-doped fiber laser (YDFL) operating at ~1 μm . The cavity of such lasers may be ring or linear with broadband or fixed-wavelength reflection, e.g., by a pair fiber Bragg gratings (FBG) resonant to a chosen Stokes wavelength. At cascaded generation, multiple FBG pairs resonantly reflect

all Stokes components from the first to the highest order that goes to the output [2], but the FBG losses limit the efficiency of cascaded generation in such schemes. Recently, an FBG-free linear scheme of cascaded RFL based on randomly distributed feedback (RDFB) via Rayleigh backscattering has been demonstrated, enabling almost loss-less cascaded Raman conversion with efficiency close to the quantum limit, e.g., the absolute optical efficiency of pump-to-highest-order-Stokes conversion reaches 88%, 75% and 70% for the first, second and third Stokes, respectively [3–5]. At the same time, the use of a special Raman fiber with high gain and shifted zero dispersion wavelength together with a broadband half-open cavity with RDFB allows for the cascaded generation with quasi-continuous wavelength tuning in a nearly octave spanning range from ~ 1 to ~ 1.9 μm [6]. The only drawback of all RFL schemes based on single-mode passive fibers is that they need a single-mode high-power fiber laser pumping source such as YDFL, whereas conventional fiber lasers (and YDFL itself) employ quite simple and reliable high-power multimode laser diode (LD) pumping.

Recently, a direct LD pumping in RFL scheme was successfully implemented in telecom multimode graded-index fibers (GIF) [7–9]; see also [10,11] for a review of the main results obtained. It appears possible to efficiently convert highly multimode LD radiation into a Stokes beam with improved beam quality and brightness, thanks to the Raman beam cleanup effect arising from the specific transverse structure of SRS gain in graded-index fibers [12,13]. Recent implementation of special FBGs inscribed by femtosecond pulses in the central part of the GIF core (of 62.5 μm diameter) enables the generation of a Stokes beam with nearly diffraction-limited quality [14]. The highest brightness enhancement factor of 73 has been obtained at the conversion of highly multimode ($M^2 \sim 34$) pump LD radiation at ~ 940 nm into a Stokes radiation at 976 nm with $M^2 < 2$ and power > 50 W in 100 μm GIF [13,15]. Together with fiber-based combining and coupling of the pump radiation of several LDs, such a scheme offers a new approach for high-brightness, diode-pumped, all-fiber lasers with wavelength tuning within the Raman gain bandwidth.

Here, we report on an opportunity to further broaden the operating wavelength range via cascaded Raman conversion in graded-index fibers of multimode LD pump radiation into higher Stokes orders, analyzing the results of papers [16,17] with a corresponding discussion of the key physical process and adding new results that help to clarify Raman laser operation in cascaded schemes based on multimode fibers. Linear and half-open (with RDFB) cavities for high-order Stokes generation are compared. In the optimized configuration, a sequential beam quality improvement from $M^2 \sim 34$ up to a diffraction-limited beam ($M^2 < 1.3$) for the highest order with high conversion efficiency is demonstrated.

2. Schemes of the Cascaded Raman Lasers Based on Multimode Fiber

Three CW multimode laser diodes (LD1-3) pigtailed by a step-index fiber (SIF) with a 100 μm core are combined by a pump combiner and directly pump a 1 km graded-index fiber (GIF) with a 100 μm core, thus producing Raman gain in it; see Figure 1. A resonator of the Raman laser is formed by an UV-inscribed highly reflective ($R \sim 90\%$) fiber Bragg grating (UV FBG) and a fs-inscribed output grating (FS FBG) with a low reflection coefficient ($R \sim 4\%$) at the corresponding Stokes wavelength, thus providing output coupling of the generated Stokes beam either of the first or second Stokes order. For the second Stokes order, instead of FS FBG, an angle-cleaved (~ 10 degrees) fiber end has been also tested for output coupling from the cavity. The laser output is collimated by a lens and characterized by a power meter (P), beam profiler (M^2) and optical spectrum analyzer (OSA), with the use of corresponding interference filters (IF) for selection of either the pump or the first and second Stokes beams. Two different LD sets with wavelengths of 915 or 940 nm with a total input power in GIF up to ~ 200 W have been used for pumping. The corresponding conversion of highly multimode ($M^2 \sim 34$) pump radiation at 915 nm into the first/second Stokes waves with wavelengths 950 (954)/976 (996) nm selected by corresponding FBG sets have been explored in the first case [16], and 940 nm LD pump conversion into the first/second Stokes waves with wavelengths 976/1019 nm in the second case [17].

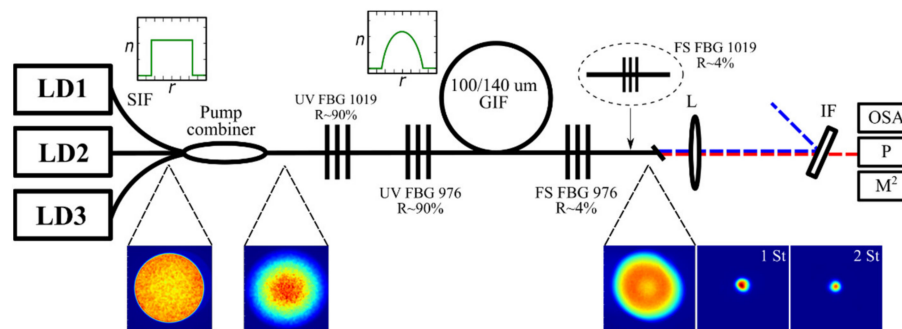


Figure 1. Cascaded Raman laser scheme based on multimode LD-pumped fiber: LD1-3 are laser diodes pigtailed by step-index fiber (SIF) with 100 μm core and combined by a pump combiner; GIF is 1 km Raman graded-index fiber with 100 μm core in which an UV-inscribed highly reflective ($R\sim 90\%$) fiber Bragg grating (UV FBG) and a fs-inscribed output coupler ($R\sim 4\%$) (FS FBG) form a cavity at wavelengths corresponding to the 1st and the 2nd Stokes waves. The laser output is collimated by a lens and characterized by a power meter (P), beam profiler (M^2) and optical spectrum analyzer (OSA), with the use of corresponding interference filters (IF) for selection of either the pump or the 1st and 2nd order Stokes beams. Pump beam profiles measured before and after pump combiner in SIF and GIF, respectively, and after FS FBG, are shown together with the generated 1st and 2nd Stokes beam shapes.

Beam cross-sections for the multimode 940 nm LD pump radiation measured before and after the pump combiner in SIF and GIF, respectively, and after FS FBG, are shown together with the generated first (976 nm) and second (1019 nm) Stokes beam shape at the output. One can see that a significant reduction in the output beam size and corresponding improvement in the beam quality M^2 occurs at each stage of the pump to the first and second Stokes beam conversion. This improvement is mainly defined by the mode-selective properties of fs-inscribed FBGs, in which the modified refractive index is localized in a small area of $1 \times 8 \mu\text{m}$ near the GIF core center, thus providing predominant reflection of the fundamental mode; see [18] for more details. The reflection spectra of the 976 and 1019 nm FBG pairs employed in the scheme with 940 nm pump LDs are shown in Figure 2a,b. One can see that the fs-inscribed (FS) low-reflection (LR) FBG has the main long-wavelength peak corresponding to the fundamental mode, whereas shorter-wavelength peaks corresponding to higher-order transverse modes are lower by ~ 10 dB. Note that in the case of high-reflection (HR) FBGs, the CW UV light modifies a significant part of the Ge-doped fiber core so that the difference between the main short-wavelength reflection peak corresponding to the fundamental mode and short-wavelength peaks corresponding to higher-order modes amounts to a few dB only. The obtained output characteristics in different cavity configurations are shown in the next sections.

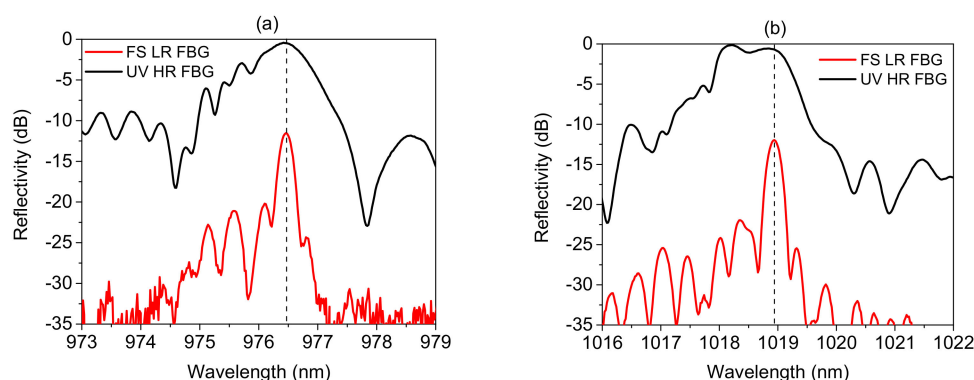


Figure 2. Reflection spectra of FBG pairs: UV-inscribed high-reflection (HR) FBG and FS-inscribed low-reflection (LR) FBG used as cavity mirrors for the 1st Stokes wave at ~ 976 nm (a) and for the 2nd Stokes wave at 1019 nm (b) at ~ 940 nm LD pumping.

3. Output Power/Efficiency in Different Schemes

As a first step, we compared cascaded generation in a linear cavity formed by highly reflective UV FBG and a mode-selective FS FBG with low reflection ($R \sim 4\%$) for both the first (S1) and the second (S2) Stokes wave—see Figure 3a—with the configuration in which output FS FBG for the second Stokes wave is absent so that it starts generating in a half-open cavity configuration due to the random distributed feedback via Rayleigh backscattering; see Figure 3b. We tested [16,17] and compare here two different wavelength sets—(1) 940 nm (LD)–976 nm (S1)–1019 nm (S2); (2) 915 nm (LD)–950 nm (S1)–976 nm (S2)—which show similar behavior. Although the generation threshold is lower in the case of the linear RFL cavity for the second Stokes wave (Figure 3a), the slope efficiency for the second Stokes generation is higher in the case of the half-open random RFL (RRFL) cavity approaching approximately 37% and 43% for wavelength sets (1) and (2), respectively (Figure 3b). Note that the second Stokes wavelength in case (2) sufficiently deviates from the corresponding Raman gain maximum (it is near 992 nm in the case of 950 nm 1st Stokes wavelength, whereas at 976 nm, the Raman gain coefficient is ~ 2 times lower [16]); therefore, the generation threshold is shifted to higher pump powers in this case. Note that the maximum transmitted first Stokes power increases in configurations with the higher second Stokes threshold, whereas it behaves similarly in all cases below the second threshold. Above the second Stokes threshold, the transmitted first Stokes power is depleted more rapidly in the case of the RRFL cavity (Figure 3b) in correspondence with the higher power and slope efficiency of the second Stokes generation in this case. This means that in the multimode fiber cavity with high losses, the optimal output reflection coefficient is closer to that for random Rayleigh backscattering, estimated to be more than one order of magnitude lower than that for FS FBG with $R \sim 4\%$. However, a more precise optimization of the output coupling may further increase the second Stokes output power in this configuration.

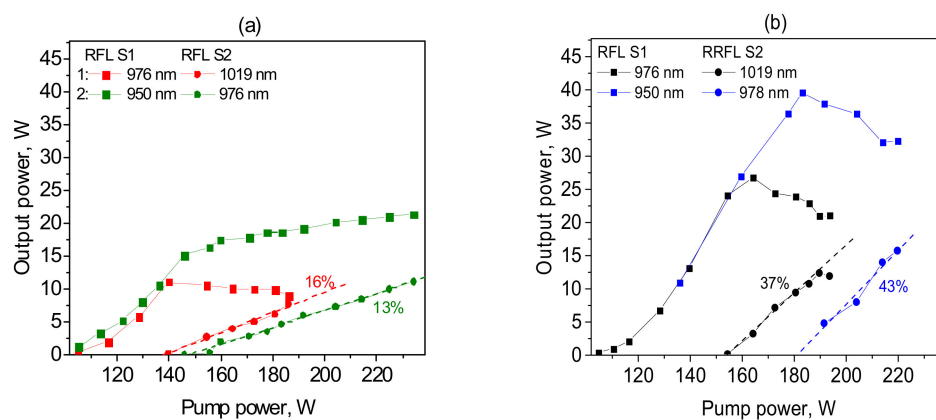


Figure 3. Output power in linear RFL cavity (a) and half-open random RFL (RRFL) cavity (b) for the 2nd Stokes wave (S2) while 1st Stokes (S1) has linear RFL cavity in two different configurations: (1) 940 nm LD pumping and 976/1019 nm S1/S2 cavity; (2) 915 nm LD pumping and 950/978 nm S1/S2 cavity, respectively.

To test the wavelength tuning possibilities around the Stokes gain maximum, we compared different FBG sets in configuration (2) with 915 nm pumping and a half-open RRFL cavity for the second Stokes wave; see Figure 4. The wavelength of the first FBG pair is shifted from 950 to 954 nm and the second HR FBG from 978 to 996 nm, exactly to the maxima of Raman gain for the first and second Stokes waves (Stokes shift corresponding to the maximum Raman gain amounts to $440\text{--}445\text{ cm}^{-1}$ in $100\text{ }\mu\text{m}$ GIF [16]). Since the difference in the first Stokes shifts is small, the two cases exhibit nearly the same first Stokes generation threshold and slope efficiency, whereas the maximum output power and slope efficiency for the second Stokes generation are sufficiently larger in the case of exact resonance corresponding to 996 nm. At the optimal conditions, the threshold value decreases and the slope efficiency of the second Stokes wave generation at 996 nm approaches that for the first Stokes wave generation (below the second threshold), amounting

to around 70% and reaching a maximum power of 27 W, comparable to that for the first Stokes wave. Meanwhile, second Stokes generation at 978 nm (shifted by $\sim 140 \text{ cm}^{-1}$ from the Raman gain maximum) exhibits around 17 W maximum power with higher threshold pump power and lower slope efficiency.

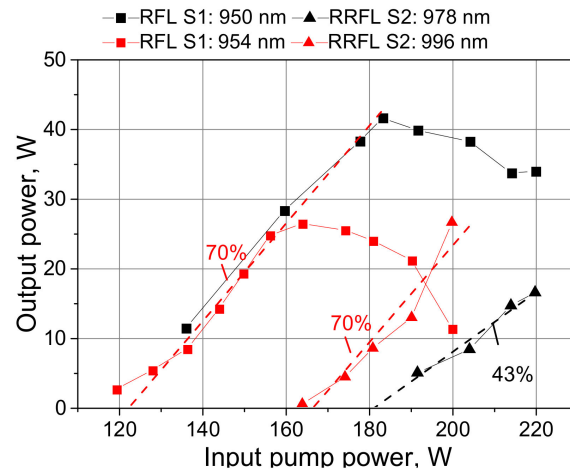


Figure 4. Measured output power of the 1st (squares) and the 2nd (triangles) Stokes waves versus multimode 915 nm LD pump power [16] coupled to the 100 μm GIF with linear cavity for the 1st Stokes wave (RFL) and half-open cavity for the 2nd Stokes random RFL (RRFL) versus the input multimode LD pump power at 915 nm at different FBG sets: HR UV FBG + OC FS FBG (RFL) at 950 nm (S1) and HR UV FBG (RRFL) at 978 nm (S2) marked in black; HR UV FBG + OC FS FBG (RFL) at 954 nm (S1) and HR UV FBG (RRFL) at 996 nm (S2) marked in red.

Let us compare the best results obtained for the cascaded Raman lasers with multimode 100 μm GIF pumped by 915 and 940 nm multimode LDs and second Stokes output at 996 and 1019 nm, respectively. The results obtained at nearly exact resonances for the first and second Stokes waves provided by the linear RFL and half-open RRFL cavity, correspondingly, are summarized for both configurations in Figure 5.

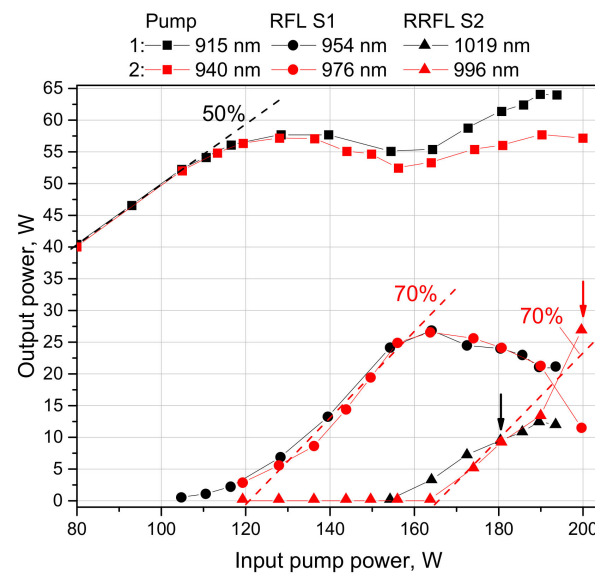


Figure 5. Transmitted pump power (squares) and output power for the 1st Stokes, S1 (circles), and 2nd Stokes, S2 (triangles), as a function of the input pump power from multimode LDs in two configurations: 915 nm LD/954 nm RFL S1/996 nm RRFL S2 (red) and 940 nm LD/976 nm RFL S1/1019 nm RRFL S2 (black). Arrows mark corresponding 3rd Stokes threshold.

The comparison shows similar qualitative behavior for both configurations, with only a slight difference in power values. In both cases, the transmitted pump power grows nearly linearly with a slope of $\sim 50\%$ up to the first Stokes threshold, amounting to 105–110 W of input power. Above the threshold, the transmitted pump power starts to saturate and even to decrease, while the first Stokes power rapidly grows with a linear trend of slope efficiency to $\sim 70\%$ for both configurations. When the second Stokes threshold is approached, the first Stokes output starts to saturate and then decreases with increasing second Stokes power. At the same time, the residual pump power starts growing again above the second Stokes threshold. The second Stokes threshold amounts to 155–165 W of input pump power; above the threshold, the second Stokes power grows near linearly in both cases with similar slope, but around 180 W of input pump power, the slope becomes different in the two configurations. For the 996 nm output, it remains high enough ($\sim 70\%$), whereas for the 1019 nm, output it slows down to $\sim 40\%$. We reveal that this slowing down is reasoned by the appearance of the third Stokes wave in this case. We identified that the low third Stokes threshold is reasoned by 1065 nm radiation coming from the pump 940 nm LDs; see [17] for more details.

4. Output Spectra in Different Schemes

The measured output spectra of the second Stokes generation at 1019 nm in the RFL and RRFL cavity configurations are compared in Figure 6a. One can see that the RFL spectra represent a relatively narrow single peak with exponential tails, which weakly broaden with increasing output power. At the same time, the RRFL spectra represent two peaks with unstable shape, which significantly broaden with increasing power. In Figure 6b, the RFL and RRFL widths at the -3 dB and -10 dB levels are compared, showing a principal difference in the width values and their dependence on power. The full width at half-maximum (-3 dB) at power ~ 10 W amounts to around 0.15 nm and 0.55 nm, respectively. The difference is mainly reasoned by the single and double peak structure of the RFL and RRFL spectra, correspondingly. In their turn, the laser spectra are defined by the reflection spectra of cavity FBGs; see Figure 2b. In RRFL, the output narrowband FS FBG is absent and both reflection peaks of the broadband UV FBG take part in Raman generation, whereas adding narrowband FS FBG in the RFL configuration selects only one peak, thus leading to the laser spectrum narrowing and stabilization. Thus, the second Stokes spectral power density in the case of RFL is higher than that for RRFL. Note that in the case of 978 nm second Stokes generation in the RRFL cavity, the UV FBG has a single reflection peak, similar to the UV FBG spectrum shown in Figure 2a. As a result, the generated RRFL spectrum narrows to a single peak (Figure 6c), with the bandwidth decreased to around 0.2 nm at 14 W, which is comparable to the RFL bandwidth, which may be treated as a method for spectral power density enhancement for RRFL. At the same time, some fluctuations (especially near the top of the spectrum) remain.

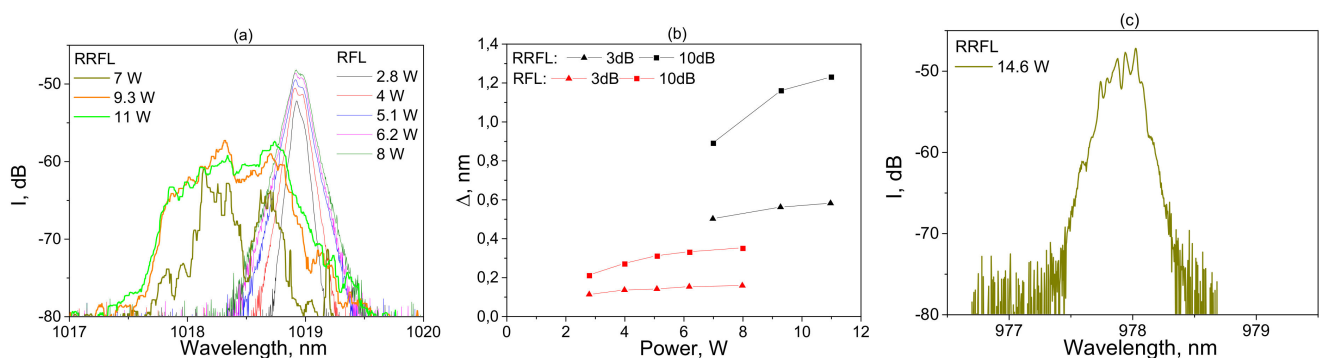


Figure 6. Comparison of spectral shapes (a) and linewidths (b) at -3 dB and -10 dB levels for RFL and RRFL 2nd Stokes generation at 1019 nm. (c) Spectral shape of RRFL 2nd Stokes generation at 978 nm.

5. Beam Profiles and Quality (M^2)

The input and transmitted pump beam and the generated first- and second-order Stokes beams were characterized in terms of beam quality parameter M^2 and beam shape by a Thorlabs M^2 -MS by using appropriate interference filters (IF) to select the corresponding wavelength. For measurement of the detailed output beam shape, we adjusted the focus on the fiber end facet given that the defocusing from the optimal focus point blurred the spatial details of the measured beam profile; for more details, see [13] and citations therein.

The measured 2D projections of the beam intensity distributions are shown at corresponding points of the scheme in Figure 1 with 940 nm LD, 976 nm and 1019 nm first- and second-order Stokes beams, respectively. The pump beam from individual LDs homogeneously fills the core of the SIF pigtail, with a transverse intensity profile similar to the index profile (the measured beam quality parameter is $M^2 \sim 26$). There are only weak signs of speckles, because of the large bandwidth (~ 5 nm) of LD radiation. After the mixing of three LD pumps in the fiber pump combiner, and propagation in ~ 2 m of GIF, the pump beam quality slightly degrades ($M^2 \sim 30$), whereas its transverse intensity profile takes a parabolic shape, mimicking the GIF index profile. This results from strong random mode coupling, leading to an equipartition of pump energy among all of the transverse modes [13]. The transmitted pump beam is also nearly parabolic ($M^2 \sim 34$), but above the Raman threshold, it becomes depleted (with a hole in the center), owing to the first Stokes beam generation (its quality parameter M^2 changes from 1.7 to 1.9 with increasing Stokes power). The second Stokes beam generated after reaching its threshold is even narrower than the first Stokes beam (its quality parameter is $M^2 = 1.3 - 1.4$ depending on power and cavity configuration being very close for RFL and RRFL cavities). Note that the better beam quality in the case of the 1019 nm second Stokes wavelength than that for 996 nm ($M^2 \sim 1.6$) may also lead to the lower slope efficiency together with the lower third Stokes threshold in this case (see Figure 5).

The beam profiles extracted from the 2D projections depending on power are shown in Figure 7. The output pump beam profile changes from a parabolic to a near-rectangular profile above the first Stokes threshold; then, a dip is formed due to the inhomogeneous pump depletion at high-power Stokes generation (but the pump dip is broader than the first Stokes beam, which is reasoned by the strong influence of random mode coupling on the pump beam; see [13] for more details). The first Stokes beam has a near-Gaussian shape defined by the FBG spatial filtering [13], and it is almost unchanged with increasing its power and even when the second Stokes beam is generated, which, in turn, is Gaussian, growing without shape changes. At the same time, above the second Stokes threshold, the transmitted pump starts growing in amplitude, with the shape of the dip kept unchanged.

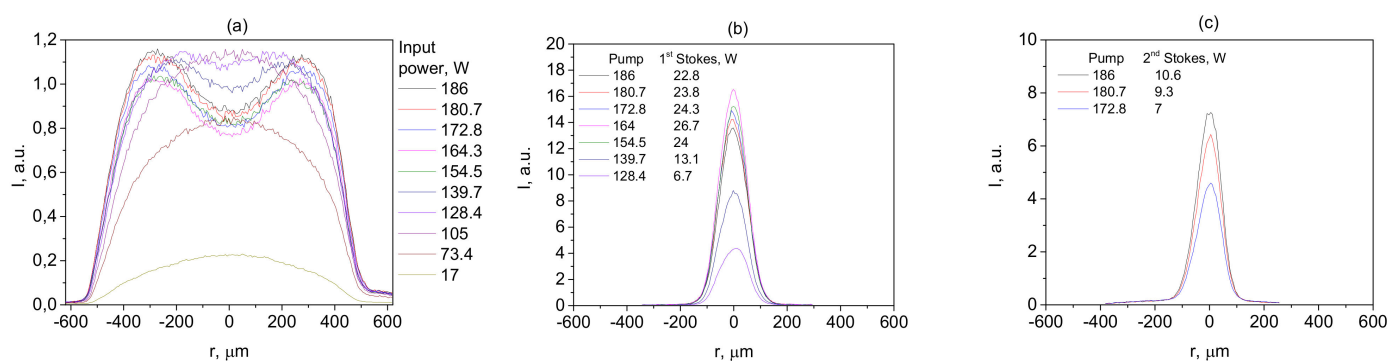


Figure 7. Beam profiles for the transmitted pump beam (a) and generated 1st (b) and 2nd (c) Stokes beams in RRFL cavity configuration as a function of power.

6. Discussion and Conclusions

Let us summarize the obtained results. In the studied system, highly multimode ($M^2 \sim 30$) 940 nm LD pump radiation up to ~ 200 W power coupled through a fiber pump combiner to a 100 μm core graded-index fiber is serially converted into the first, second and third Stokes beam. A linear cavity composed of fiber Bragg gratings (FBGs) inscribed in the fiber core is formed to provide feedback for the first Stokes order, whereas for the second order, both the linear cavity consisting of two FBGs and the half-open cavity with one FBG and random distributed feedback (RDFB) via Rayleigh backscattering along the fiber are explored. LDs with different wavelengths (915 and 940 nm) are used for pumping, enabling Raman lasing at different wavelengths of the first (950, 954 and 976 nm), second (976, 996 and 1019 nm) and third (1065 nm) Stokes orders. Output power and efficiency, spectral line shapes and widths, beam quality and shapes are compared for different configurations. It is shown that the random DFB cavity of the Raman fiber laser (RRFL) provides higher slope efficiency of the second Stokes generation than that for the conventional RFL cavity; see Figure 3. At the wavelength corresponding to the maximum Raman gain, the slope efficiency reaches 70% (close to that for the first Stokes wave) with output power up to ~ 30 W being limited by the third Stokes generation; see Figure 5. Tuning within the broadband Stokes gain profile of the second Stokes by ~ 20 nm from the wavelength corresponding to maximum gain is demonstrated with the power reduction by factor 1.6; see Figure 4.

While the quality parameter M^2 for the first Stokes beam at maximum power is close to 2, the beam quality parameter of the second Stokes beam approaches the diffraction limit ($M^2 \sim 1.3$) in the case of the 1019 nm wavelength both in the linear and half-open cavities, whereas the line is narrower (< 0.2 nm) and more stable for the linear cavity with two FBGs; see Figure 6. However, an optimization of the FBG reflection spectrum used in the half-open cavity allows this linewidth value to be approached, but the line shape in the case of the RRFL cavity remains less stable than that for RFL. In both cases, the measured beam profiles show the dip formation in the output pump beam, whereas the first and second Stokes beams are Gaussian-shaped and almost unchanged with increasing power; see Figure 7. The qualitative explanation of such behavior in connection with the power evolution of the transmitted pump and generated first, second and third Stokes beams may be given on the basis of the power balance model, similar to that for single-mode cascaded RFL [19]. When the input pump power reaches the first Stokes threshold, the transmitted pump power starts to saturate and then decreases, while the first Stokes power grows nearly linearly; see Figure 5. When it reaches the second Stokes threshold, the pump power starts increasing again in order to compensate for the additional losses of the first Stokes wave power because of its conversion into the second Stokes wave. At the same time, the first Stokes power starts to decrease. When the second Stokes wave reaches the third Stokes threshold, the first Stokes output in turn starts increasing in order to compensate for the losses due to the conversion of the second Stokes wave into the third Stokes wave. Looking at the beam profiles (Figure 7), the depletion of the highly multimode pump beam occurs inhomogeneously, whereas nearly single-mode first and second beams evolve without significant changes in the beam shapes, which are close to Gaussian. Thus, considering an averaging over transverse modes, the interaction of pump and Stokes components in the multimode case is similar to that for single-mode RFL [19].

In conclusion, the treated scheme of the multimode cascaded Raman fiber laser represents a new type of LD-pumped fiber laser source that has the advantage of wavelength agility in comparison with conventional LD-pumped fiber lasers such as rare-earth-doped fiber lasers. It may generate in a broad wavelength range defined by available high-power multimode LDs. With the use of commercially available 9xx nm LDs, it is able to generate at almost any wavelength in the 950–1020 nm range, where the generation of conventional fiber lasers has serious limitations, such as photo-darkening [20]. Consequently, wavelength tuning may be performed by means of both cascaded generation of the higher Stokes orders and detuning from the Raman gain maximum within the bandwidth of

individual Stokes order (first or second). At the cascaded conversion, the beam quality is gradually improved to $M^2 < 2$ (1st Stokes) and $M^2 < 1.4$ (2nd Stokes) due to the Raman beam cleanup effect supported by the mode-selective properties of cavity FBGs [13] or Rayleigh backscattering (RBS) in graded-index fibers. Herewith, the use of random DFB via RBS in an half-open cavity with one FBG for the second Stokes order allows one to increase its output power (~30 W) and slope efficiency (~70%) to the level characteristic for the first Stokes order. The third Stokes generation at ~1065 nm is shown to be also achievable, but this wavelength range is not so interesting as it is covered by a high-power Yb-doped fiber laser [20]. Further development of multimode LD-pumped cascaded RFLs may be focused on their power scaling similarly to the first-order RFL [21] and towards a shorter wavelength operation range with the use of 8xx nm high-power LDs.

The developed sources may find their application in biomedical diagnostics in the spectral range of <1 micron, frequency doubling [22] to the spectral range of <500 nm and potential use in laser displays, frequency quadrupling to the spectral range of <250 nm and specific UV applications. The potential for wavelength tuning may also increase the application range, e.g., by the development of fiber-based sources that are alternative to the tunable systems based on Ti:Sa lasers.

Author Contributions: Conceptualization, S.A.B.; methodology, A.G.K., E.A.E. and S.I.K.; investigation A.G.K., I.N.N., A.A.W. and E.A.E.; data and analysis, A.G.K., E.A.E. and S.I.K.; writing, A.G.K., S.I.K. and S.A.B.; project administration and funding acquisition, S.A.B. All authors have read and agreed to the published version of the manuscript.

Funding: The work is supported by the Russian Science Foundation (grant 21-72-30024).

Institutional Review Board Statement: Not applicable.

Informed Consent Statement: Not applicable.

Data Availability Statement: The data that support the findings of this study are available from the corresponding author upon reasonable request.

Conflicts of Interest: There are no conflicts to declare.

References

1. Dianov, E.M.; Prokhorov, A.M. Medium-power CW Raman fiber lasers. *IEEE J. Sel. Top. Quantum Electron.* **2000**, *6*, 1022–1028. [[CrossRef](#)]
2. Supradeepa, V.R.; Feng, Y.; Nicholson, J.W. Raman fiber lasers. *J. Opt.* **2017**, *19*, 023001. [[CrossRef](#)]
3. Zlobina, E.A.; Kablukov, S.I.; Babin, S.A. Linearly polarized random fiber laser with ultimate efficiency. *Opt. Lett.* **2015**, *40*, 4074–4077. [[CrossRef](#)]
4. Du, X.; Zhang, H.; Wang, X.; Zhou, P.; Liu, Z. Short cavity-length random fiber laser with record power and ultrahigh efficiency. *Opt. Lett.* **2016**, *41*, 571. [[CrossRef](#)] [[PubMed](#)]
5. Babin, S.A.; Zlobina, E.A.; Kablukov, S.I.; Podivilov, E.V. High-order random Raman lasing in a PM fiber with ultimate efficiency and narrow bandwidth. *Sci. Rep.* **2016**, *6*, 22625. [[CrossRef](#)] [[PubMed](#)]
6. Zhang, L.; Jiang, H.; Yang, X.; Pan, W.; Cui, S.; Feng, Y. Nearly-octave wavelength tuning of a continuous wave fiber laser. *Sci. Rep.* **2017**, *7*, 42611. [[CrossRef](#)]
7. Kablukov, S.I.; Dontsova, E.I.; Zlobina, E.A.; Nemov, I.N.; Vlasov, A.A.; Babin, S.A. An LD-pumped Raman fiber laser operating below 1 μm . *Laser Phys. Lett.* **2013**, *10*, 085103. [[CrossRef](#)]
8. Yao, T.; Harish, A.; Sahu, J.; Nilsson, J. High-Power Continuous-Wave Directly-Diode-Pumped Fiber Raman Lasers. *Appl. Sci.* **2015**, *5*, 1323–1336. [[CrossRef](#)]
9. Glick, Y.; Fromzel, V.; Zhang, J.; Dahan, A.; Ter-Gabrielyan, N.; Pattnaik, R.K.; Dubinskii, M. High power, high efficiency diode pumped Raman fiber laser. *Laser Phys. Lett.* **2016**, *13*, 065101–065106. [[CrossRef](#)]
10. Babin, S.A.; Zlobina, E.A.; Kablukov, S.I. Multimode Fiber Raman Lasers Directly Pumped by Laser Diodes. *IEEE J. Sel. Top. Quantum Electron.* **2018**, *24*, 1–10. [[CrossRef](#)]
11. Glick, Y.; Shamir, Y.; Sintov, Y.; Goldring, S.; Pearl, S. Brightness enhancement with Raman fiber lasers and amplifiers using multi-mode or multi-clad fibers. *Opt. Fiber Technol.* **2019**, *52*, 101955. [[CrossRef](#)]
12. Terry, N.B.; Alley, T.G.; Russell, T.H. An explanation of SRS beam cleanup in graded-index fibers and the absence of SRS beam cleanup in step-index fibers. *Opt. Express* **2007**, *15*, 17509. [[CrossRef](#)] [[PubMed](#)]
13. Kuznetsov, A.G.; Kablukov, S.I.; Podivilov, E.V.; Babin, S.A. Brightness enhancement and beam profiles in an LD-pumped graded-index fiber Raman laser. *OSA Contin.* **2021**, *4*, 1034. [[CrossRef](#)]

14. Zlobina, E.A.; Kablukov, S.I.; Wolf, A.A.; Dostovalov, A.V.; Babin, S.A. Nearly single-mode Raman lasing at 954 nm in a graded-index fiber directly pumped by a multimode laser diode. *Opt. Lett.* **2017**, *42*, 9. [[CrossRef](#)]
15. Kuznetsov, A.G.; Kablukov, S.I.; Wolf, A.A.; Nemov, I.N.; Tyrtysnyy, V.A.; Myasnikov, D.V.; Babin, S.A. 976 nm all-fiber Raman laser with high beam quality at multimode laser diode pumping. *Laser Phys. Lett.* **2019**, *16*, 105102. [[CrossRef](#)]
16. Evmenova, E.A.; Kuznetsov, A.G.; Nemov, I.N.; Wolf, A.A.; Dostovalov, A.V.; Kablukov, S.I.; Babin, S.A. 2nd-order random lasing in a multimode diode-pumped graded-index fiber. *Sci. Rep.* **2018**, *8*, 17495. [[CrossRef](#)] [[PubMed](#)]
17. Kuznetsov, A.G.; Nemov, I.N.; Wolf, A.A.; Kablukov, S.I.; Babin, S.A. Multimode LD-pumped all-fiber Raman laser with excellent quality of 2nd -order Stokes output beam at 1019 nm. *Opt. Express* **2021**, *29*, 17573. [[CrossRef](#)]
18. Dostovalov, A.V.; Wolf, A.A.; Skvortsov, M.I.; Abdullina, S.R.; Kuznetsov, A.G.; Kablukov, S.I.; Babin, S.A. Femtosecond-pulse inscribed FBGs for mode selection in multimode fiber lasers. *Opt. Fiber Technol.* **2019**, *52*, 101988. [[CrossRef](#)]
19. Babin, S.A.; Churkin, D.V.; Podivilov, E. V Intensity interactions in cascades of a two-stage Raman fiber laser. *Opt. Commun.* **2003**, *226*, 329–335. [[CrossRef](#)]
20. Richardson, D.J.; Nilsson, J.; Clarkson, W.A. High power fiber lasers: Current status and future perspectives [Invited]. *J. Opt. Soc. Am. B* **2010**, *27*, B63–B92. [[CrossRef](#)]
21. Fan, C.; Chen, Y.; Yao, T.; Xiao, H.; Xu, J.; Leng, J.; Zhou, P.; Wolf, A.A.; Nemov, I.N.; Kuznetsov, A.G.; et al. Over 400 W graded-index fiber Raman laser with brightness enhancement. *Opt. Express* **2021**, *29*, 19441. [[CrossRef](#)] [[PubMed](#)]
22. Kuznetsov, A.G.; Evmenova, E.A.; Dontsova, E.I.; Kablukov, S.I.; Babin, S.A. Frequency doubling of multimode diode-pumped GRIN-fiber Raman lasers. *Opt. Express* **2019**, *27*, 34760. [[CrossRef](#)] [[PubMed](#)]